Two New Quadrilateral Elements Based on Strain States

Rezaiee-Pajand, M.[1*] and Yaghoobi, M.[2]

[1] Professor, Civil Engineering Department, Ferdowsi University of Mashhad, Mashhad, Iran

[2] Ph.D. Candidate, Civil Engineering Department, Ferdowsi University of Mashhad, Mashhad, Iran

Abstract: In this paper, two new quadrilateral elements are formulated to solve plane problems. Low sensitivity to geometric distortion, no parasitic shear error, rotational invariance, and satisfying the Felippa pure bending test are characteristics of these suggested elements. One proposed element is formulated by establishing equilibrium equations for the second-order strain field. The other suggested element is obtained by establishing equilibrium equations only for the linear part of the strain field. The number of the strain states decreases when the conditions among strain states are satisfied. Several numerical tests are used to demonstrate the performance of the proposed elements. Famous elements, which were suggested by other researchers, are used as a means of comparison. It is shown that these novel elements pass the strong patch tests, even for extremely poor meshes, and one of them has an excellent accuracy and fast convergence in other complicated problems.

INTRODUCTION

Free formulation was first based on kinematics decomposition. Free formulation indicates that the basic part fulfills convergence of the finite element. Felippa (2006) set up the correct rank of the stiffness matrix and increased accuracy using the high-order part. Strain gradient notation creates a suitable space to find the error of the finite element pattern using a Taylor series expansion of the strain field. This scheme adequately specifies shear locking and parasitic shear error. In other words, the slopes of the strains point to the root of many finite element modeling errors (Dow, 1999).

The parameterized variational principle in the formulation of finite element technique changed the science of high-performance elements. In this way,

scientists could define the continuous space of an elastic functional. Making the continuous space of the functional stationary produces free parameters for formulation of the element, creating finite element templates (Felippa and Militello, 1990). Further investigation revealed that the template formulations followed specific and identical structures. There was no need to make the parametrized functional stationary to obtain these templates. Assigning values to the free parameters of these templates provides the various elements (Felippa, 2000). Optimization of finite element templates is difficult, however, and requires innovation. The large number of free parameters, symbolic processing and matrix structure optimization are difficulties faced by researchers who study the templates.

Strain gradient notation is a simple and clear demonstration of free formulation. An efficient element of SSQUAD (strain

---

* Corresponding author Email: mrpajand@yahoo.com

state quadrilateral element) was recently proposed using strain gradient notation and free formulation (Rezaiee-Pajand and Yaghoobi, 2012). In this element, the optimization constraints of insensitivity to distortion, rotational invariance and absence of parasitic shear error were employed. It was evident that a complete selection of strain states from each order satisfies all three conditions. In addition, the need to establish an optimization constraint for bending in the linear strain states was identified in the formulation. Entering the states of rigid body motion is a convergence criterion of the formulation. To fulfill this condition, a linear strain field is used for the SSQUAD element.

Equilibrium allowed establishment of equations among the strain states. Consequently, two strain states could be written in terms of other strain states. This decreased the number of the strain states required in the formulation. Equilibrium equations for formulation of the SSQUAD element increased the performance of the element. It should be noted that hybrid stress elements satisfy equilibrium conditions in a strong form (Santos and Moitinho de Almeida, 2014). As will be demonstrated, completely satisfying the equilibrium equation does not produce more accurate responses. In fact, using the rotational degree of freedoms and satisfying equilibrium in second-order filed decrease the ability of the suggested element. To eliminate this weakness, equilibrium should be satisfied in the linear displacement field.

Severe numerical tests display fast convergence and insensitivity to distortion in the mesh for the SSQUAD element. This element, like other good elements, such as AGQ6-II, provides answers with large error in strong patch tests for constant stress and bending with bilinear stress for high distortion (Prathap and Senthilkumar, 2008).

The present study uses high-order fields and imperfectly establishes equilibrium equations to eliminate the weakness of the SSQUAD element in the strong patch tests of constant stress and bending with bilinear stress for high distortion. Selecting a complete second-order strain field satisfies optimization constraints for insensitivity to geometric distortion, absence of parasitic shear error, and rotational invariance. The new element also satisfies Felippa's pure bending test. To apply a second-order strain field, 20 strain states are needed to present the element.

Satisfying the equilibrium equations is explored using perfect and imperfect types. The SSQ14 element (strain state quadrilateral element with 14 DOF) is obtained by setting up perfect equilibrium equations for the second-order strain field. The SSQ18 element (strain state quadrilateral element with 18 DOF) is obtained by employing equilibrium equations only for the linear part of the strain field. Relationships among the strain states are created using equilibrium equations. In the new formulation, these equations decreases the number of required strain states for SSQ14 and SSQ18 to 14 and 18, respectively.

The proposed formulations are based on Taylor's expansion of the strain field. Several optimal constraints are included to obtain errorless responses. The equilibrium conditions are satisfied, to some extent, using only the constant parts of the strains. The proposed strategy provides two simple elements that pass the patch test and work efficiently, even in coarse distorted meshes.

These types of elements are innovative, and their performance is examined using a variety of numerical tests. The responses to high-quality elements of other researchers are also used as a means of comparison. Section 4.1 explains the improved performance of SSQ18 and SSQ14 elements over other good elements, such as SSQUAD and AGQ6-II. The SSQ18 element also demonstrates superior accuracy and fast convergence in other tests.

Optimization Constraints

A formulation that allows optimization is required to obtain efficient elements. The proposed strategy demonstrates the roots of many errors. Sufficient constraints must be a component of any formulation to improve performance. The following subsections explain the constraints used in the proposed technique.

In-plane pure bending test

Felippa used this test to find the optimum bending template (Felippa, 2003, 2004, 2006). He examined the responses of the template for in-plane bending by evaluating the energy ratios using an Euler-Bernoulli beam where r_x and r_y denote the bending energy ratios of a rectangular part of the beam in the x and y directions, respectively. If $r_x = 1$, $r_y = 1$, or $r = 1$, the element can model flexure in an arbitrary direction. If $r > 1$ or $r < 1$, the element is either over-stiff or over-flexible. For each aspect ratio of element $r = 1$, the element is at flexural optimum. In the case of insensitivity to the aspect ratio, r increases, and the element will experience shear locking.

When this test is based on strain states and in-plane bending occurs in the x direction, the real stress field changes linearly in the y direction. The strain field for this case is based on the Hooke's law as follows:

$$\varepsilon_x = \beta_1 + \beta_2 y \quad , \quad \varepsilon_y = \beta_3 + \beta_4 y \quad , \quad \gamma_{xy} = 0 \quad (1)$$

where β_1, β_2, β_3 and β_4: are constant coefficients and Eq. (1) shows that only $(\varepsilon_{y,y})_\circ$, $(\varepsilon_{x,y})_\circ$, $(\varepsilon_y)_\circ$ and $(\varepsilon_x)_\circ$ strain states exist in this field. For bending in the y direction, the real strain field includes $(\varepsilon_{y,x})_\circ$, $(\varepsilon_{x,x})_\circ$, $(\varepsilon_y)_\circ$ and $(\varepsilon_x)_\circ$ strain states. To obtain the real answer for in-plane bending, $(\varepsilon_{y,y})_\circ$, $(\varepsilon_{y,x})_\circ$, $(\varepsilon_{x,y})_\circ$, $(\varepsilon_{x,x})_\circ$, $(\varepsilon_y)_\circ$ and $(\varepsilon_x)_\circ$ strain states must be used.

$(\varepsilon_x)_\circ$: is the magnitude of axial strain ε_x at the origin, $(\varepsilon_{x,x})_\circ$, and $(\varepsilon_{x,y})_\circ$ are the rate of ε_x variations in x and y directions, in the vicinity of origin, respectively. Other coefficients are also determined by using a similar tactic.

The existence of constant strain states and rigid body motions in the assumed strain field of the element is a convergence criterion and must exist in all cases. The bending test based on strain states has no limitation for geometric shape or type of mesh. It covers elements other than the triangular and quadrilateral elements.

Rotational invariance

The properties of some elements change if the coordinate axes rotate. These elements are not rotational invariant. An element having different rotated shapes in the mesh of the structure inevitably requires rotational invariance. Rotational invariance depends on the complete selection of expressions of the strain field of each order (Dow, 1999).

Absence of parasitic shear error

The appearance of axial strain states in shear strain interpolation polynomial creates parasitic shear error, which leads to hardening of the element (Dow, 1999). Shear strains, including Taylor series shear strain, are independent of axial strain. In the shear strain interpolation function of elements with parasitic shear error, some axial strain states incorrectly appear. If such an element experiences flexural deformation, the axial strain states are non-zero and are erroneously representative of part of the shear strain. In elements formulated using strain gradient notation, the parasitic shear error can be eliminated by setting aside the spurious strain states from the shear strain polynomial. Parasitic shear error decreases as the mesh becomes finer. Despite this, if an element is free of error, coarse mesh will also produce correct answers. It should be noted that the

selection of the complete strain interpolation functions prevents the appearance of this error.

Equilibrium conditions

In formulation of the SSQUAD element, setting up the equilibrium equations increases the performance of the element and decreases the number of strain states. By selecting a complete polynomial from each order, inclusion of parasitic shear and the rotational variance errors can be prevented.

The linear strain field was used to formulate the SSQUAD element. SSQ14 and SSQ18 were formulated using a complete second-order strain field. By selecting this field, rotational invariance and absence of parasitic shear error are guaranteed. It is evident that this field can satisfy the Felippa pure bending test. The difference between SSQ14 and SSQ18 is in the establishment of equilibrium equations. In the SSQ14 element, complete equilibrium equations are set up; in the SSQ18 element, the equilibrium equations are satisfied for the linear part of the strain field.

The present study shows the superiority of the case in which the equilibrium equations are partially fulfilled. For the strain field of the complete second order, 20 nodal unknowns are needed. For the full and partial establishment of the equilibrium equations, 6 and 2 strain states, respectively, are written in terms of other strain states. The equilibrium equations inside an elastic homogeneous element for in-plane stress or strain become:

$$\begin{cases} \dfrac{\partial \sigma_x(x,y)}{\partial x} + \dfrac{\partial \tau_{xy}(x,y)}{\partial y} + F_x(x,y) = 0 \\ \dfrac{\partial \tau_{xy}(x,y)}{\partial x} + \dfrac{\partial \sigma_y(x,y)}{\partial y} + F_y(x,y) = 0 \end{cases} \quad (2)$$

where σ_x, σ_y and τ_{xy}: are stresses at any point on the element, and $F_x(x,y)$ and $F_y(x,y)$: are force fields inside the element in the x and y directions, respectively, in a Cartesian coordinate system.

In plane problems, it is evident that the variation of the force field in the direction normal to the element plane (z direction here) does not exist. The stress fields are selected in the Cartesian coordinate system. Based on the Hooke's law for a homogeneous elastic state, Eq. (2) can be written as:

$$\sigma_x = 2G\varepsilon_x + \lambda(\varepsilon_x + \varepsilon_y) \quad (3)$$

$$\sigma_y = 2G\varepsilon_y + \lambda(\varepsilon_x + \varepsilon_y) \quad (4)$$

$$\tau_{xy} = G\gamma_{xy} \quad (5)$$

$$\begin{cases} (2G+\lambda)\dfrac{\partial \varepsilon_x(x,y)}{\partial x} + \lambda\dfrac{\partial \varepsilon_y(x,y)}{\partial x} \\ + G\dfrac{\partial \gamma_{xy}(x,y)}{\partial y} + F_x(x,y) = 0 \\ \lambda\dfrac{\partial \varepsilon_x(x,y)}{\partial y} + (2G+\lambda)\dfrac{\partial \varepsilon_y(x,y)}{\partial y} \\ + G\dfrac{\partial \gamma_{xy}(x,y)}{\partial x} + F_y(x,y) = 0 \end{cases} \quad (6)$$

The λ for plane stress and plane strain states are $\dfrac{vE}{(1+v)(1-v)}$ and $\dfrac{vE}{(1+v)(1-2v)}$, respectively, and G, v, and E: are elasticity parameters of shear modulus, Poisson's ratio and Young's modulus, respectively.

SSQ14 and SSQ18

The formulation of the SSQ14 and SSQ18 elements is described below based on the assumed strain functions.

SSQ14

The formulation of SSQ14 and SSQ18 employs the strain and displacement fields as:

$$\begin{cases} \mathbf{u}_x = (\mathbf{u}_x)_\circ + (\varepsilon_x)_\circ x + (\gamma_{xy}/2 - r_r)_\circ y + (\varepsilon_{x,x})_\circ x^2/2 + (\varepsilon_{x,y})_\circ xy + (\gamma_{xy,y} - \varepsilon_{y,x})_\circ y^2/2 \\ + (\varepsilon_{x,xx})_\circ x^3/6 + (\varepsilon_{x,xy})_\circ x^2 y/2 + (\varepsilon_{x,yy})_\circ y^2 x/2 + (\gamma_{xy,yy} - \varepsilon_{y,xy})_\circ y^3/6 \\ \mathbf{u}_y = (\mathbf{u}_y)_\circ + (\gamma_{xy}/2 + r_r)_\circ x + (\varepsilon_y)_\circ y + (\gamma_{yx,x} - \varepsilon_{x,y})_\circ x^2/2 + (\varepsilon_{y,x})_\circ xy + (\varepsilon_{y,y})_\circ y^2/2 \\ + (\gamma_{xy,xx} - \varepsilon_{x,xy})_\circ x^3/6 + (\varepsilon_{y,xx})_\circ x^2 y/2 + (\varepsilon_{y,xy})_\circ y^2 x/2 + (\varepsilon_{y,yy})_\circ y^3/6 \end{cases} \quad (7)$$

$$\begin{cases} \varepsilon_x(x,y) = (\varepsilon_x)_\circ + (\varepsilon_{x,x})_\circ x + (\varepsilon_{x,y})_\circ y + (\varepsilon_{x,xx})_\circ x^2/2 + (\varepsilon_{x,xy})_\circ xy + (\varepsilon_{x,yy})_\circ y^2/2 \\ \varepsilon_y(x,y) = (\varepsilon_y)_\circ + (\varepsilon_{y,x})_\circ x + (\varepsilon_{y,y})_\circ y + (\varepsilon_{y,xx})_\circ x^2/2 + (\varepsilon_{y,xy})_\circ xy + (\varepsilon_{y,yy})_\circ y^2/2 \\ \gamma_{xy}(x,y) = (\gamma_{xy})_\circ + (\gamma_{xy,x})_\circ x + (\gamma_{xy,y})_\circ y + (\gamma_{xy,xx})_\circ x^2/2 + (\varepsilon_{x,yy} + \varepsilon_{y,xx})_\circ xy + (\gamma_{xy,yy})_\circ y^2/2 \end{cases} \quad (8)$$

In Eq. (8), the coefficient of xy: is $(\varepsilon_{x,yy} + \varepsilon_{y,xx})_\circ$. This is derived from the strains compatibility condition, which is $(\gamma_{xy,xy})_\circ = (\varepsilon_{x,yy})_\circ + (\varepsilon_{y,xx})_\circ$. The formulation of SSQ14 satisfies the equilibrium equations completely; thus, the strain field in Equation (8) is substituted into Eq. (6). In equilibrium equations, the body forces of $F_x(x, y)$ and $F_y(x, y)$ are ignored. As a result, the relationship among the strain states is:

$$\begin{cases} (\gamma_{xy,x})_\circ = (-\frac{\lambda}{G})(\varepsilon_{x,y})_\circ - (\frac{2G+\lambda}{G})(\varepsilon_{y,y})_\circ \\ (\gamma_{xy,y})_\circ = (-\frac{\lambda}{G})(\varepsilon_{y,x})_\circ - (\frac{2G+\lambda}{G})(\varepsilon_{x,x})_\circ \\ (\gamma_{xy,xx})_\circ = (-\frac{\lambda}{G})(\varepsilon_{x,xy})_\circ - (\frac{2G+\lambda}{G})(\varepsilon_{y,xy})_\circ \\ (\gamma_{xy,yy})_\circ = (-\frac{\lambda}{G})(\varepsilon_{y,xy})_\circ - (\frac{2G+\lambda}{G})(\varepsilon_{x,xy})_\circ \\ (\varepsilon_{x,xx})_\circ = (-\frac{G+\lambda}{2G+\lambda})(\varepsilon_{y,xx})_\circ - (\frac{G}{2G+\lambda})(\varepsilon_{x,yy})_\circ \\ (\varepsilon_{y,yy})_\circ = (-\frac{G+\lambda}{2G+\lambda})(\varepsilon_{x,yy})_\circ - (\frac{G}{2G+\lambda})(\varepsilon_{y,xx})_\circ \end{cases} \quad (9)$$

The number of unknowns in the formulation has now decreased to 14. The formulation is carried out using the 14 residual strain states and the vector of the strain states is:

$$\hat{q}^T = \big[(u_x)_\circ \ (u_y)_\circ \ (r_r)_\circ \ (\varepsilon_x)_\circ \ (\varepsilon_y)_\circ \ (\gamma_{xy})_\circ \ (\varepsilon_{x,x})_\circ$$
$$(\varepsilon_{x,y})_\circ \ (\varepsilon_{y,x})_\circ \ (\varepsilon_{y,y})_\circ \ (\varepsilon_{x,xy})_\circ \ (\varepsilon_{x,yy})_\circ \ (\varepsilon_{y,xy})_\circ \ (\varepsilon_{y,xx})_\circ \big] \quad (10)$$

The displacements and strains are transformed to the next matrix as:

$$\mathbf{U} = \hat{\mathbf{N}}_q \cdot \hat{\mathbf{q}} \quad (11)$$

$$\hat{N}_q = \begin{bmatrix} 1 & 0 & -y & x & 0 & \frac{y}{2} & \frac{x^2}{2} - \frac{(2G+\lambda)y^2}{2G} \\ 0 & 1 & x & 0 & y & \frac{x}{2} & 0 \end{bmatrix}$$

$$xy \qquad -\frac{(G+\lambda)y^2}{2G} \qquad 0$$
$$-\frac{(G+\lambda)x^2}{2G} \qquad xy \qquad \frac{y^2}{2} - \frac{(2G+\lambda)x^2}{2G}$$
$$\frac{x^2 y}{2} - \frac{(2G+\lambda)y^3}{6G} \quad \frac{y^2 x}{2} - \frac{G x^3}{12G+6\lambda}$$
$$-\frac{(G+\lambda)x^3}{6G} \qquad -\frac{(G+\lambda) y^3}{12G+6\lambda}$$
$$-\frac{(G+\lambda)y^3}{6G} \qquad -\frac{(G+\lambda) x^3}{12G+6\lambda}$$
$$\frac{y^2 x}{2} - \frac{(2G+\lambda) x^3}{6G} \quad \frac{x^2 y}{2} - \frac{G y^3}{12G+6\lambda} \quad (12)$$

$$\boldsymbol{\varepsilon} = \hat{\mathbf{B}}_q \cdot \hat{\mathbf{q}} \quad (13)$$

$$\hat{B}_q = \begin{bmatrix} 0 & 0 & 0 & 1 & 0 & 0 & x \\ 0 & 0 & 0 & 0 & 1 & 0 & 0 \\ 0 & 0 & 0 & 0 & 0 & 1 & -\frac{(2G+\lambda)}{G}y \end{bmatrix}$$

$$y \qquad 0 \qquad 0$$
$$0 \qquad x \qquad y$$
$$-\frac{\lambda}{G}x \quad -\frac{\lambda}{G}y \quad -\frac{(2G+\lambda)}{G}x$$
$$xy \qquad \frac{y^2}{2} - \frac{G}{(4G+2\lambda)}x^2$$
$$0 \qquad -\frac{(G+\lambda)}{(4G+2\lambda)}y^2$$
$$-\frac{\lambda}{2G}x^2 - \frac{(2G+\lambda)}{2G}y^2 \qquad xy$$
$$0 \qquad -\frac{(G+\lambda)}{(4G+2\lambda)}x^2$$
$$xy \qquad \frac{x^2}{2} - \frac{G}{(4G+2\lambda)}y^2$$
$$-\frac{\lambda}{2G}y^2 - \frac{(2G+\lambda)}{2G}x^2 \qquad xy \qquad (14)$$

SSQ18

The displacement and strain fields of Eqs. (7) and (8) are used in the formulation of the SSQ18 element. Equilibrium equations (Eq. (6)) are set up for the linear part of the strain field in Eq. (8). As a result, $(\gamma_{xy,x})_\circ$ and $(\gamma_{xy,y})_\circ$ are written in terms of other strain states.

$$\begin{cases} (\gamma_{xy,x})_\circ = (-\dfrac{\lambda}{G})(\varepsilon_{x,y})_\circ - (\dfrac{2G+\lambda}{G})(\varepsilon_{y,y})_\circ \\ (\gamma_{xy,y})_\circ = (-\dfrac{\lambda}{G})(\varepsilon_{y,x})_\circ - (\dfrac{2G+\lambda}{G})(\varepsilon_{x,x})_\circ \end{cases}$$
(15)

The number of the unknowns has now decreased to 18 and the formulation is performed for the 18 residual strain states. The vector of the strain states is:

$$\hat{q}^T = \big[(u_x)_\circ \ (u_y)_\circ \ (r_r)_\circ \ (\varepsilon_x)_\circ \ (\varepsilon_y)_\circ \ (\gamma_{xy})_\circ$$
$$(\varepsilon_{x,x})_\circ \ (\varepsilon_{x,y})_\circ \ (\varepsilon_{y,x})_\circ \ (\varepsilon_{y,y})_\circ \ (\varepsilon_{x,xx})_\circ \ (\varepsilon_{x,xy})_\circ$$
$$(\varepsilon_{x,yy})_\circ \ (\varepsilon_{y,xx})_\circ \ (\varepsilon_{y,xy})_\circ \ (\varepsilon_{y,yy})_\circ \ (\gamma_{xy,xx})_\circ \ (\gamma_{xy,yy})_\circ \big]$$
(16)

The $\hat{\mathbf{N}}_q$ and $\hat{\mathbf{B}}_q$ matrices are:

$$\hat{N}_q = \begin{bmatrix} 1 & 0 & -y & x & 0 & \dfrac{y}{2} & \dfrac{x^2}{2} - \dfrac{(2G+\lambda)y^2}{2G} \\ 0 & 1 & x & 0 & y & \dfrac{x}{2} & 0 \\ xy & & -\dfrac{(G+\lambda)y^2}{2G} & & & & 0 \\ -\dfrac{(G+\lambda)x^2}{2G} & & xy & & \dfrac{y^2}{2} - \dfrac{(2G+\lambda)x^2}{2G} & & \\ \dfrac{x^3}{6} & \dfrac{x^2y}{2} & \dfrac{y^2x}{2} & 0 & -\dfrac{y^3}{6} & 0 & 0 & \dfrac{y^3}{6} \\ 0 & -\dfrac{x^3}{6} & 0 & \dfrac{x^2y}{2} & \dfrac{y^2x}{2} & \dfrac{y^3}{6} & \dfrac{x^3}{6} & 0 \end{bmatrix}$$
(17)

$$\hat{B}_q = \begin{bmatrix} 0 & 0 & 0 & 1 & 0 & 0 & x & y & 0 \\ 0 & 0 & 0 & 0 & 1 & 0 & 0 & 0 & x \\ 0 & 0 & 0 & 0 & 0 & 1 & -\dfrac{(2G+\lambda)}{G}y & -\dfrac{\lambda}{G}x & -\dfrac{\lambda}{G}y \\ 0 & \dfrac{x^2}{2} & xy & \dfrac{y^2}{2} & 0 & 0 & 0 & 0 & 0 \\ y & 0 & 0 & 0 & \dfrac{x^2}{2} & xy & \dfrac{y^2}{2} & 0 & 0 \\ -\dfrac{(2G+\lambda)}{G}x & 0 & 0 & xy & xy & 0 & 0 & \dfrac{x^2}{2} & \dfrac{y^2}{2} \end{bmatrix}$$
(18)

Degrees of freedom

SSQ14 and SSQ18 elements have 14 and 18 DOF, respectively. The arrangements of the DOF of the two elements are shown in Figure 1.
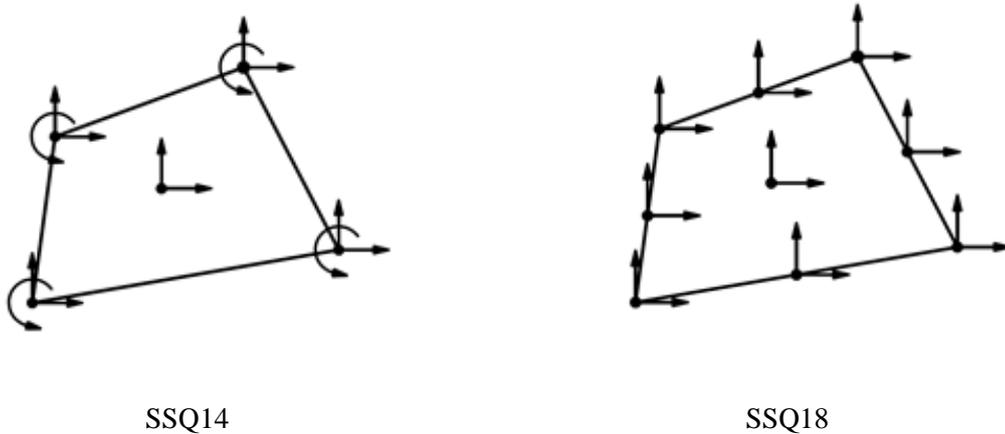

SSQ14

SSQ18

Fig. 1. The degrees of freedom for SSQ14 and SSQ18 elements.

Finding the stiffness matrix

By allotting $\hat{\mathbf{N}}_q$, $\hat{\mathbf{B}}_q$, and $\hat{\mathbf{q}}$ matrices for each SSQ14 and SSQ18 element, their stiffness matrices can be found. The displacement unknowns are denoted by the vector of the strain states ($\hat{\mathbf{q}}$). The nodal DOF are denoted by vector D. The relationship $\mathbf{U} = \hat{\mathbf{N}}_q \cdot \hat{\mathbf{q}}$ holds between the displacement functions in the x and y directions, **U**, and the displacement unknowns ($\hat{\mathbf{q}}$). The nodal rotations are defined as $\frac{1}{2}(\frac{\partial u_y}{\partial x} - \frac{\partial u_x}{\partial y})$. The nodal displacements are the shifts in the x and y directions plus the nodal rotation. The following equations connect the nodal DOF and the displacement unknowns:

$$\mathbf{D} = \hat{\mathbf{G}}_q \cdot \hat{\mathbf{q}} \tag{19}$$

$$\hat{\mathbf{q}} = \hat{\mathbf{G}}_q^{-1} \cdot \hat{\mathbf{D}} \tag{20}$$

The $\hat{\mathbf{G}}_q$ matrix is obtained by inserting the nodal coordinates of each element into the corresponding $\hat{\mathbf{N}}_q$ and sets up the relation between the vector of the strain states and the nodal displacement vector. Consequently, the displacement boundary conditions can be entered into the formulation. The displacement and strain fields for the nodal displacement vector in matrix form are:

$$\mathbf{U} = \hat{\mathbf{N}}_q \cdot \hat{\mathbf{q}} = \hat{\mathbf{N}}_q \cdot (\hat{\mathbf{G}}_q^{-1} \cdot \hat{\mathbf{D}}) = \mathbf{N} \cdot \hat{\mathbf{D}} \tag{21}$$

$$\boldsymbol{\varepsilon} = \hat{\mathbf{B}}_q \cdot \hat{\mathbf{q}} = \hat{\mathbf{B}}_q \cdot (\hat{\mathbf{G}}_q^{-1} \cdot \hat{\mathbf{D}}) = \mathbf{B} \cdot \hat{\mathbf{D}} \tag{22}$$

where $\mathbf{N} = \hat{\mathbf{N}}_q \cdot \hat{\mathbf{G}}_q^{-1}$ and $\mathbf{B} = \hat{\mathbf{B}}_q \cdot \hat{\mathbf{G}}_q^{-1}$. The functional of the potential energy for the elasticity matrix of **E** is:

$$\boldsymbol{\Pi} = \frac{1}{2} \int \varepsilon^T \cdot \mathbf{E} \cdot \varepsilon \, dv - \int U^T \cdot \mathbf{F} \, dv$$

$$= \frac{1}{2} \hat{D}^T (\int B^T \cdot E \cdot B \, dv) \hat{D} - \hat{D}^T \int N^T \cdot F \, dv \tag{23}$$

Optimization of the potential energy results in:

$$\frac{\partial \boldsymbol{\Pi}}{\partial \hat{\mathbf{D}}} = \mathbf{0} \tag{24}$$

$$\frac{\partial \boldsymbol{\Pi}}{\partial \hat{\mathbf{D}}} = (\int \mathbf{B}^T \cdot \mathbf{E} \cdot \mathbf{B} \, dv) \hat{\mathbf{D}} - \int \mathbf{N}^T \cdot \mathbf{F} \, dv = \mathbf{0} \tag{25}$$

This equation can be expressed as:

$$(\int \mathbf{B}^T \cdot \mathbf{E} \cdot \mathbf{B} \, dv) \hat{\mathbf{D}} = \int \mathbf{N}^T \cdot \mathbf{F} \, dv \tag{26}$$

Stiffness matrix **K** and nodal load vector **P** are:

$$\mathbf{K} = \int \mathbf{B}^T \cdot \mathbf{E} \cdot \mathbf{B} \, dv \tag{27}$$

$$\mathbf{P} = \int \mathbf{N}^T \cdot \mathbf{F} \, dv \tag{28}$$

The shape function matrices are defined by **N**. Analytical schemes are used to find the stiffness matrix. Using triangular coordinates, the quadrilateral element is divided into two triangular shapes and the stiffness matrix is easily integrated.

NUMERICAL TESTS

The abilities of the proposed elements were evaluated using 12 difficult test problems. To demonstrate the power of new formulation, the answers of the good elements of other researchers were used for comparison. These elements are:
• 4-node isoparametric element: Q4 (Chen et al., 2004; Wisniewski and Turska, 2009)
• Element with internal parameters formulated by QACM-I: AGQ6-II (Cen et al., 2009; Chen et al., 2004)
• Element with internal parameters formulated by QACM-I: QACM4 (Cen et al., 2007)
• Quadrilateral element in MSC/NASTRAN: CQUAD4 (Choi et al., 2006; MacNeal, 1971)
• 4-node isoparametric element with internal parameters: HL (Bergan and Felippa, 1985; Cook, 1974)

- Stress hybrid element: PS (Cen et al., 2009; Chen et al., 2004; Pian and Sumihara, 1984)
- Triangular element with rotational DOF: $FF_{(\alpha=1.5, \beta=0.5)}$ (Bergan and Felippa, 1985)
- Allman's element: ALLMAN (Allman, 1984; Choo et al., 2006; Cook, 1986)
- Membrane element with drilling DOF: Q4S (Cen et al., 2009; MacNeal and Harder, 1988)
- Hybrid element with internal parameters: NQ6 (Cen et al., 2009; Wu et al., 1987)
- Non-conforming isoparametric element with internal parameters: QM6 (Cen et al., 2009; Chen et al., 2004; Choi et al., 2006; Taylor et al., 1976)
- Non-conforming isoparametric element with internal parameters: Q6 (Cen et al., 2007, 2009; Wilson et al., 1973)
- Ibrahimbegovic plane element with true rotation: IB (Choi et al., 2006; Ibrahimgovic et al., 1990)
- Membrane element with drilling DOF: D-type (Cen et al., 2009; Ibrahimgovic et al., 1990)
- Hybrid Trefftz plane element: HT (Choo et al., 2006; Jirousek and Venkatesh, 1992)
- Assumed strain element: PEAS7 (Andelfinger and Ramm, 1993; Chen et al., 2004)
- Modified enhanced assumed strain element: MEAS (Choi et al., 2006; Choo et al., 2006; Yeo and Lee, 1997)
- Quadrilateral element with two enhanced strain modes: QE-2 (Cen et al., 2009; Piltner and Taylor, 1995, 1997)
- Assumed strain element: B-Q4E (Cen et al., 2009; Piltner and Taylor, 1997)
- Quadrilateral hybrid Trefftz element with rotational DOF: HTD (Choo et al., 2006)
- HR element with 5 modes in skew coordinates: HR5-S (Wisniewski and Turska, 2006, 2009)

- Enhanced assumed displacement gradient element with 4 modes: EADG4 (Wisniewski and Turska, 2008, 2009)
- Mixed 4-node elements based on Hu-Washizu functional: HW12-S, HW14-S, HW10-N, HW14-N, HW18 (Wisniewski and Turska, 2009)
- Free formulation quadrilateral: FFQ (Felippa, 2003; Nygard, 1986)
- 4-node membrane elements with analytical element stiffness matrix: QAC-ATF4 (Cen et al., 2009)
- 8-node membrane element based on 3 quadrilateral area coordinate methods QACM-I, -II, and -III: CQAC-Q8 (Long et al., 2010)
- 8-node element formulated using quadrilateral area coordinates: QACM8 (Cen et al., 2007)
- Conventional 8-node quadrilateral isoparametric elements: Q8
- Hybrid stress element using first Piola–Kirchhoff stresses of degree 4 and displacements of degree 2: Hybrid stress element with $d_p=4$, $d_v=2$ (Santos and Moitinho de Almeida, 2014)

Cantilever Beam with Distortion Parameter

The cantilever beam shown in Figure 2 has two elements, the shapes of which vary with the variation of distorted parameter *e*. The existence of coarse mesh, an aspect ratio of 2.5 for $e = 0$ and intense distortions in the mesh make it an appropriate test for evaluating the sensitivity of the distortion of the mesh. The modulus of elasticity is 75, Poisson's ratio is 0.25, and thickness of the structure is 1.

Figure 3 shows analysis of the cantilever beam under 3 loadings at the free end of the beam. This structure has an axial force of 1 at the free end of the beam for the constant stress patch test. For the bending patch test with linear stress, a moment equal to 1 is applied to the free end of the beam. A shear load equal to 1 is

applied to the free end of the structure for the bending patch test with bilinear stress.

The displacements of the proposed elements at A for each loading and for different magnitudes of *e* are listed in Tables 1 to 3. The exact vertical displacement of point A under the bending moment is 1 and under a shear load is 6.8333. The exact horizontal displacement at point A under the axial load is 0.0667 (Prathap and Senthilkumar, 2008).

Some very good elements, such as SSQUAD and AGQ6-II, give poor results and can lead to considerable error in the patch tests for constant stress and bending with bilinear stress for poor mesh. SSQ18 and SSQ14 are proposed to obtain adequate performance in these strong patch tests, even for extremely poor mesh.
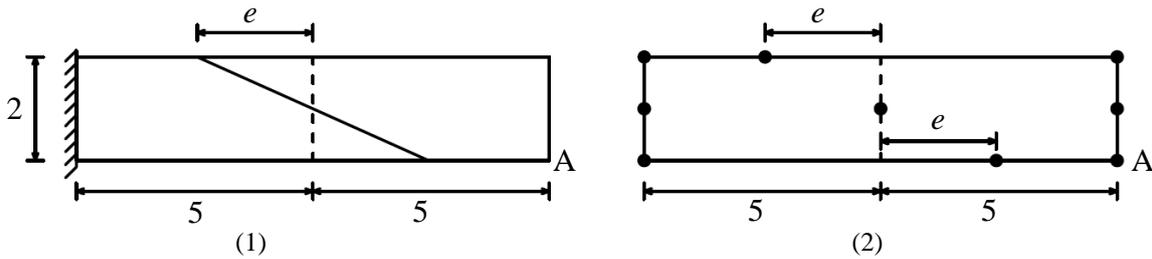

Fig. 2. The geometry of the two and one-element mesh of the cantilever beam with the distorted parameter of *e*.
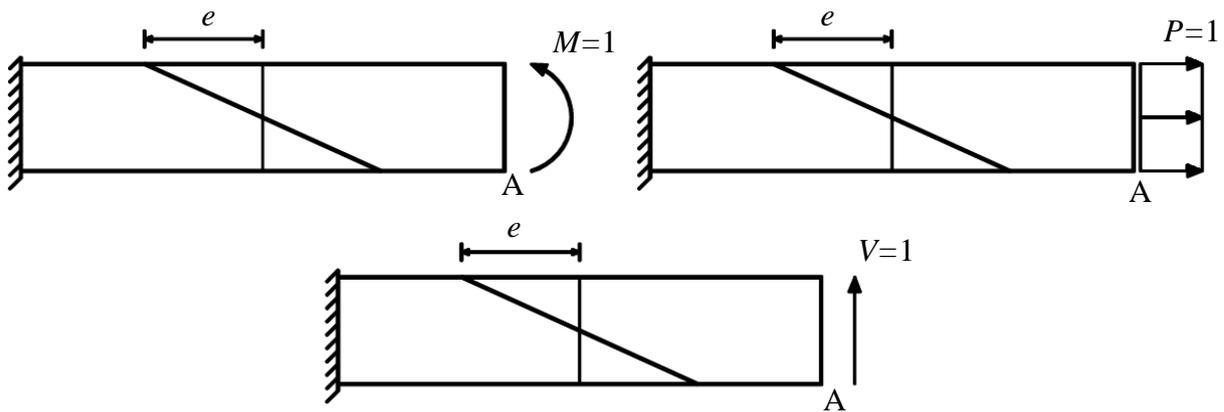

Fig. 3. The three loadings used for the cantilever beam.

Table 1. The normalized vertical displacement of point A of the cantilever beam under the bending moment.

e	0	0.5	1	2	3	4
HT	31.5	24.5	17.5	13.6	13.7	14.5
ALLMAN	93.8	95	90.7	56.7	31.8	17.9
MEAS	100	59.5	39.2	30.8	26.9	23.1
Q6	100	93.2	86.9	92.8	102.4	110.5
QM6	100	80.9	62.7	54.4	53.6	51.2
PS	100	81	62.9	55	54.7	53.1
QE2	100	81.2	63.4	56.5	57.5	57.9
B-Q4E	100	81.2	63.4	56.5	57.5	57.9
HTD	100	99.2	99.6	100.9	83.6	57.8
AGQ6-II	100	100	100	100	100	100
QACM4	100	83.8	66.5	60.1	61.4	60.3
QAC-ATF4	100	100	100	100	100	100
Q8	100	99.9	99.3	89.39	59.7	32.01
QACM8	100	100	100.2	100.7	101.9	103.7
SSQUAD	100	100	100	100	100	100
SSQ14	99.8	100	100.1	100.7	101.2	102.8
SSQ18	96.6	97.6	98.5	100.4	105.3	116.8
Exact (Prathap and Senthilkumar, 2008)	100	100	100	100	100	100

Table 2. The normalized horizontal displacement of point A of the cantilever beam under the axial load.

e	0	1	2	3	4
AGQ6-II	1.000	1.054	1.225	1.544	2.084
SSQUAD	0.991	1.046	1.218	1.540	2.082
SSQ14	1.064	1.065	1.123	1.295	1.581
SSQ18	1.002	1.010	1.014	1.014	1.014
Exact (Prathap and Senthilkumar, 2008)	1.000	1.000	1.000	1.000	1.000

Table 3. The normalized vertical displacement of point A of the cantilever beam under the shear load on the free end.

e	0	1	2	3	4
AGQ6-II	0.9396	0.9650	1.0520	1.2370	1.5916
Q8	0.9765	0.9298	0.7992	0.5478	0.3255
QACM8	0.9765	0.9483	0.8830	0.8489	0.8421
SSQUAD	0.9390	0.9635	1.0493	1.2344	1.5899
SSQ14	0.9849	0.9885	0.9948	1.0080	1.0415
SSQ18	0.9458	0.9740	0.9915	1.0284	1.1136
Exact (Prathap and Senthilkumar, 2008)	1.0000	1.0000	1.0000	1.0000	1.0000

SSQ18 showed less than 5% error in analysis of the cantilever beam under a moment for magnitudes of *e* equal to 0, 0.5, 1, 2 and 3. The errors for the beam under axial and shear loading at magnitudes of *e* equal to 4 were 1% and 11%, respectively. The errors by AGQ6-II were 108% and 59%. These outcomes demonstrate that SSQ14 results for shear and moment loading showed better accuracy than the SSQ18 results.

A cantilever beam was analyzed using SSQ18 in one-element mesh (Figure 2b). The displacement at point A by SSQ18 for V, P and M loadings and different magnitudes of *e* are listed in Table 4. These results show the insensitivity of SSQ18 to the arrangement of nodes.

MacNeal Thin Beam

This test evaluates the decrease in accuracy for parallelogram-shaped and trapezoidal mesh. Figure 4 shows a thin cantilever beam with rectangular, parallelogram-shaped and trapezoidal mesh. MacNeal suggested this benchmark for testing sensitivity to distortion in the mesh for quadrilateral elements (MacNeal and Harder, 1985). Six elements are used for analysis. The aspect ratio of the elements in the rectangular mesh is 5. Since a high aspect ratio creates distortion in the parallelogram-shaped and trapezoidal mesh, it is an appropriate test to evaluate the efficiency of the elements. The modulus of elasticity is 10000000, Poisson's ratio is 0.3 and thickness of the structure is 0.1. This problem has two types of loading; pure bending under a bending moment and bending under a shear force of one at the free end of the beam. The exact vertical displacement at point A of the free end of the beam for moment and shear loading are 0.0054 and 0.1081, respectively (Cen et al., 2009).

Table 4. The normalized displacement of point A of the cantilever beam in the one-element SSQ18 mesh (Exact solution (Prathap and Senthilkumar, 2008) is equal to 1.0000).

| Load	*e*				
	0	1	2	3	4
V	0.9442	0.9442	0.9442	0.9442	0.9442
P	0.9944	0.9944	0.9944	0.9944	0.9944
M	0.9612	0.9612	0.9612	0.9612	0.9612
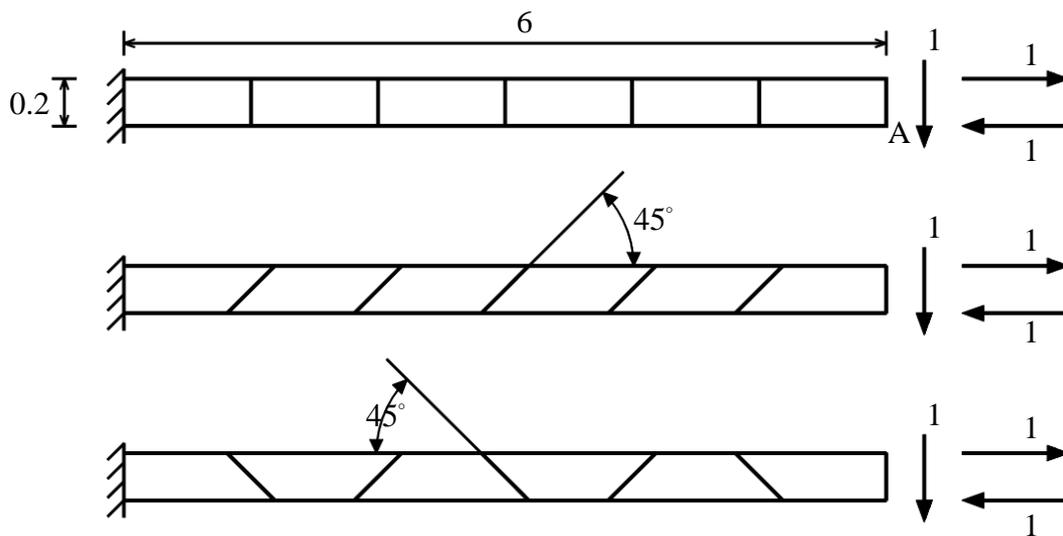
Fig. 4. The rectangular, parallelogram-shaped and trapezoidal meshes of the MacNeal beam.

Table 5 shows that for both types of loading, SSQ14 and SSQ18 in trapezoidal and parallelogram-shaped mesh showed no sensitivity to distortion. The results of other elements showed high sensitivity to distortion such that the error of the results for trapezoidal mesh increased significantly for both types of loading. SSQ18 provided an accurate response for both types of loading and for all types of mesh. Furthermore, SSQ14 showed a low error for both types of loading.

Shear Wall without Opening

SSQ14 and SSQ18 are used to analyze a cantilever shear wall without an opening. The geometry and loading of this wall is shown in Figure 5a. The elasticity modulus is 20,000,000 kN/m^2 and the structural Poisson's ratio is 0.2. Loads P and q are 100 kN and 500 kN, respectively.

The shear wall is analyzed for the types of mesh shown in Figure 5b. The lateral displacement at the top of the shear wall is calculated for the types of mesh using SSQUAD, SSQ14, SSQ18 and Q8 elements. For comparison, the opt* element was also used and its results are available elsewhere (Paknahad et al., 2007). The powerful opt* element was specifically created for analysis of shear walls.

Figure 6 shows the high accuracy of the SSQ18 element. For refined mesh, SSQ14 produced larger responses. This indicates that the rotational DOF and satisfying the equilibrium condition in the domain of the second-order field decreased the ability of SSQ14. To eliminate this weakness, the equilibrium condition was satisfied in the linear displacement field.

Shear Wall with Opening

The geometry and loading of a cantilever shear wall with an opening is shown in Figure 7a. The modulus of elasticity is 20,000,000 kN/m^2 and the Poisson's ratio is 0.25. The thickness of the wall is 0.4 m and force P is 500 kN. Two types of mesh, a and b, are used in the analysis of this shear wall (Figure 7b). SSQ14 and SSQ18 were used to calculate the lateral displacement at floor level on stories 2, 4, 6, and 8 for both types of mesh. The opt* element results were again used as a means of comparison (Paknahad et al., 2007).

The results for SSQUAD and Q8 are shown in Table 6. For assessment purposes, the results for Q8 were calculated for fine mesh for this shear wall. The shear wall was divided into 10×10 rectangular elements and the mesh denoted as c and had 26880 Q8 elements

(Paknahad et al., 2007). Table 6 shows that the responses for SSQ18 for mesh b showed minimum error. Accurate results were achieved by solving for the cantilever shear wall with an opening using SSQ18 and SSQUAD.
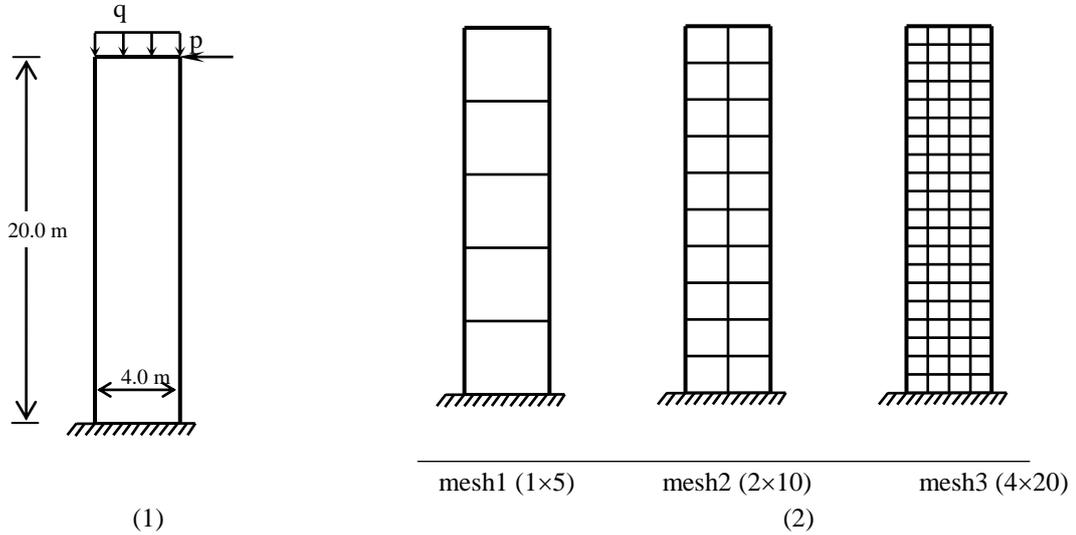

**Fig. 5.** The geometry, loading and mesh of the cantilever shear wall without opening.
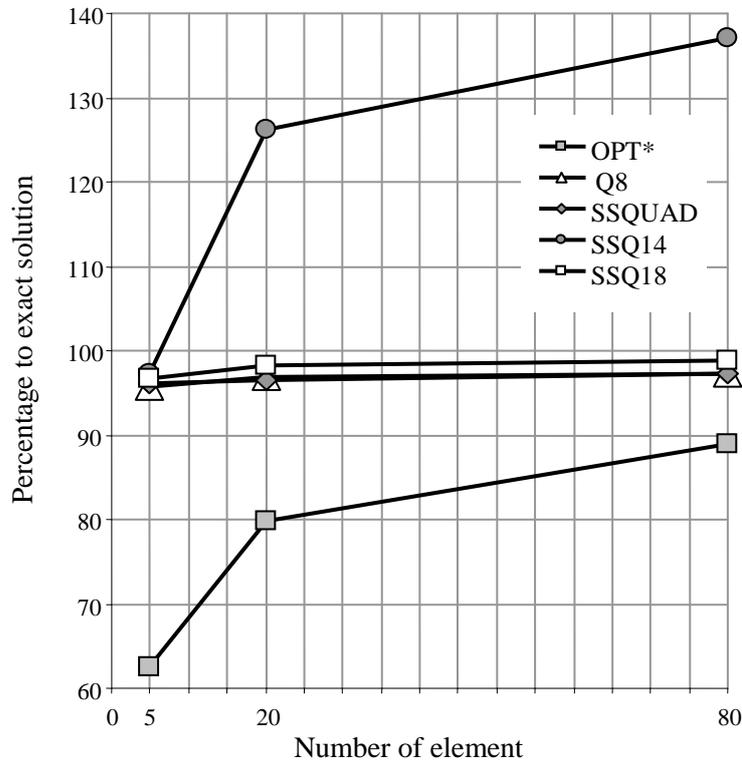
Fig. 6. The normalized lateral displacement at the top of the cantilever shear wall without opening.

Table 5. The normalized vertical displacement at point A of the MacNeal beam.

| Elements	Shear Force at Tip			Bending Moment at Free End		
	Rectangular	Parallelogram	Trapezoidal	Rectangular	Parallelogram	Trapezoidal
CQUAD4	0.600	0.632	0.051	-	-	-
ALLMAN	0.904	0.873	0.805	-	-	-
MEAS	0.993	0.621	0.044	-	-	-
Q6	0.993	0.677	0.106	1.00	0.759	0.093
QM6	0.993	0.623	0.044	1.00	0.722	0.037
PS	0.993	0.798	0.221	1.00	0.852	0.167
PEAS7	0.982	0.795	0.217	-	-	-
AGQ6-II	0.993	0.994	0.994	1.00	1.00	1.00
QACM4	0.993	0.635	0.052	1.00	0.722	0.046
QAC-ATF4	0.993	0.994	0.994	1.00	1.00	1.00
Q8	0.951	0.919	0.854	1.00	0.994	0.939
QACM8	0.951	0.903	0.895	1.00	1.00	1.00
SSQUAD	0.993	0.994	0.994	1.00	1.00	1.00
SSQ14	0.983	0.987	0.988	0.989	0.991	0.992
SSQ18	1.00	1.00	1.00	1.00	1.00	1.00
Exact (Cen et al., 2009)	1.000	1.000	1.000	1.000	1.000	1.000
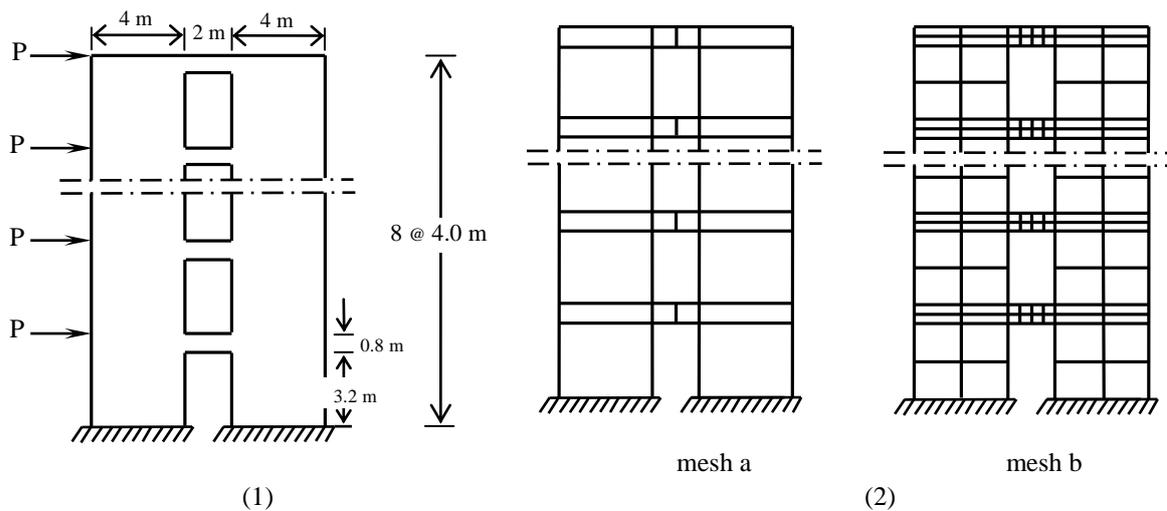
Fig. 7. The geometry, loading and meshes of the cantilever shear wall with opening.

Table 6. The lateral displacement at the levels of the floors of the 2, 4, 6, and 8 stories of the cantilever shear wall with opening.

Element	Model	Lateral Displacement at Floor Level			
		Floor 2	Floor 4	Floor 6	Floor 8
opt*	a	0.71	1.91	3.19	4.43
	b	0.74	1.98	3.28	4.51
Q8	a	0.56	1.53	2.59	3.62
	b	0.68	1.82	3.02	4.16
SSQUAD	a	0.77	2.06	3.40	4.70
	b	0.78	2.08	3.43	4.70
SSQ14	a	0.90	2.62	4.61	6.63
	b	1.14	3.22	5.49	7.70
SSQ18	a	0.76	2.03	3.36	4.61
	b	0.80	2.13	3.51	4.81
Q8	c	0.90	2.38	3.91	5.35

Cook's Beam

Cook's trapezoidal cantilever beam is used to evaluate the efficiency of the general quadrilateral elements (Cook et al., 1989). In this test, shear displacement is dominant and distorted quadrilateral elements are employed. Figure 8 shows that Cook's beam is fixed at one end and under uniformly distributed shear (P=1) at the other end. The modulus of elasticity is 1, Poisson's ratio is 1/3, and thickness of the structure is 1.

Mesh sizes of 2×2, 4×4, 8×8 and 16×16 are used for analysis. The results for deflection at point C are given in Table 7. The maximum principal stress at point A and the minimum principal stress at point B are listed in Table 8.

The results for other good elements were used for comparison. The results for GT9M8 in 64×64 mesh were similar to the exact results (Long and Xu, 1994). The high accuracy of the displacement response and stress for SSQ18 for coarse mesh demonstrates the capability of the proposed element. Table 7 indicates that

displacement of SSQ18 in 2×2 coarse mesh showed minimum error.

Results of the SSQ14 converged with larger answers when the mesh is refined. For this element, the nodal rotations were defined as $\frac{1}{2}(\frac{\partial u_y}{\partial x} - \frac{\partial u_x}{\partial y})$. This nodal rotation was unsuitable for SSQ14.

Tables 7 and 8 were used as a basis of comparison for the proposed element with the responses of the recent hybrid stress element (Santos and Moitinho de Almeida, 2014). The results for the hybrid stress element are based on the quadratic load variation and the proposed results arise on a constant distributed load. The hybrid stress element uses a fourth-order stress function and second-order displacement function. The stress field of the proposed element is linear. Appendix A provides the stress contours for the Cook trapezoidal cantilever beam. These contours are for stresses of σ_x, σ_y and τ_{xy} for a 4×4 mesh using SSQ18 and SSQ14.
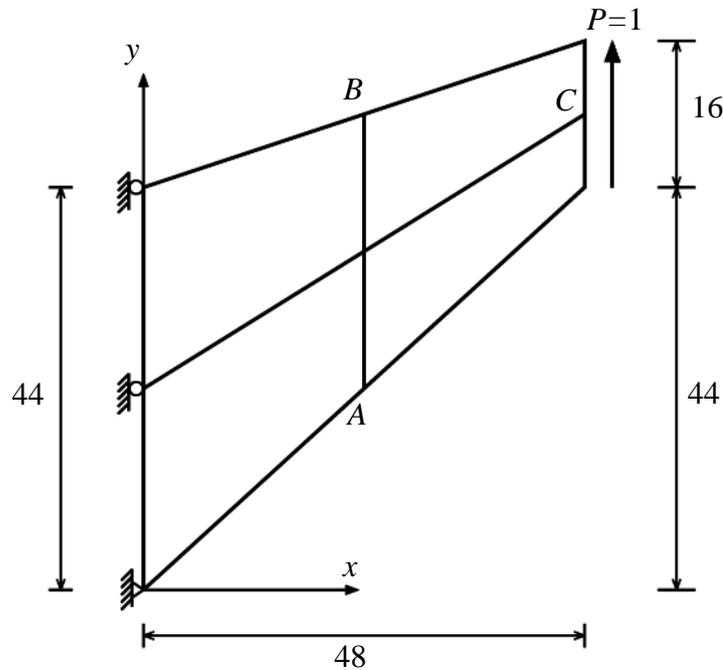

Fig. 8. The geometric properties and the loading of the Cook's beam.

Table 7. The displacement of point C of the Cook's beam.

Elements	2×2	4×4	8×8	16×16
HT	15.04	20.61	22.95	23.68
FF(α=1.5, β=0.5)	20.36	22.42	23.41	23.79
CQUAD4	21.02	23.01	23.65	23.88
ALLMAN	21.27	23.06	23.66	23.86
MEAS	21.59	23.06	23.69	23.88
FFQ	21.66	23.11	23.79	23.88
Q6	22.94	23.48	23.80	23.91
QM6	21.05	23.02	-	-
HL	18.17	22.03	-	23.81
PS	21.13	23.02	-	-
QE2	21.35	23.04	-	23.88
B-Q4E	21.35	23.04	-	23.88
HTD	23.25	23.64	23.83	23.91
AGQ6-II	25.92	24.37	24.04	23.97
QACM4	20.74	22.99	23.69	-
QAC-ATF4	24.36	23.84	23.89	-
Q8	22.72	23.71	23.88	-
QACM8	22.98	23.74	23.89	-
CQAC-Q8	22.98	23.74	23.89	-
SSQUAD	25.65	24.27	24.01	23.96
Hybrid stress element with $d_p=4$, $d_v=2$	24.53	24.21	24.16	24.15
SSQ14	27.61	30.48	31.85	32.44
SSQ18	23.45	23.70	23.86	23.92
Reference value (Long and Xu, 1994)		23.96		

Table 8. The stress answer in the Cook's beam for the 2×2, 4×4, 8×8 and 16×16 meshes.

Elements	Maximum Stress at A				Minimum Stress at B			
	2×2	4×4	8×8	16×16	2×2	4×4	8×8	16×16
HT	0.1050	0.2020	0.2280	0.2310	-0.2820	-0.2150	-0.1620	-0.1710
FF(α=1.5,β=0.5)	0.1700	0.2129	0.2309	0.2333	-0.1804	-0.1706	-0.1902	-0.1981
CQUAD4	0.1960	0.2499	0.2461	0.2422	-0.0778	-0.1672	-0.1891	-0.2062
ALLMAN	0.1600	0.2360	0.2380	0.2380	-0.2310	-0.1520	-0.1800	-0.1990
MEAS	0.1930	0.2470	0.2450	0.2410	-0.0700	-0.1760	-0.1690	-0.1790
Q6	0.2029	0.2258	0.2334	0.2361	-0.1734	-0.1915	-0.1997	-0.2028
QM6	0.1928	0.2243	-	-	-0.1580	-0.1856	-	-
HL	0.1582	0.1980	-	0.2294	-0.1335	-0.1700	-	-0.2005
PS	0.1854	0.2241	-	0.2364	-	-	-	-
QE2	0.1956	0.2261	-	0.2364	-	-	-	-
B-Q4E	0.1956	0.2261	-	0.2364	-	-	-	-
HTD	0.1720	0.2180	0.2300	0.2350	-0.2310	-0.1880	-0.1930	-0.1980
AGQ6-II	0.2169	0.2286	0.2352	0.2365	-0.1999	-0.2014	-0.2027	-0.2035
QACM4	0.1936	0.2256	0.2345	-	-0.1452	-0.1866	-0.1987	-
QAC-ATF4	0.2127	0.2277	0.2350	-	-0.1809	-0.1934	-0.2001	-
Q8	0.2479	0.2421	0.2390	-	-0.2275	-0.2007	-0.2041	-
QACM8	0.1959	0.2414	0.2389	-	-0.2142	-0.2024	-0.2041	-
CQAC-Q8	0.2523	0.2415	0.2389	-	-0.2144	-0.2024	-0.2041	-
SSQUAD	0.2137	0.2260	0.2343	0.2363	-0.1988	-0.2013	-0.2028	-0.2036
Hybrid stress element with $d_p=4$, $d_v=2$	0.2363	0.2352	0.2362	0.2367	-0.1887	-0.2058	-0.2046	-0.2038
SSQ14	0.3381	0.2976	0.2864	0.2805	-0.2596	-0.2223	-0.2054	-0.1933
SSQ18	0.2628	0.2360	0.2378	0.2373	-0.2195	-0.2014	-0.2094	-0.2047
Reference value (Long and Xu, 1994)	0.2362				-0.2023			

High-Order Patch Test

The high-order patch test uses a straight beam under pure bending. The length of the beam is 10 and the width is 1 under pure bending. Regular and distorted mesh is used to analyze the structure. Six elements are employed for each mesh. The loading and mesh of the beam is shown in Figure 9; u_x and u_y show the displacements in the x and y directions, respectively. Maximum displacement is listed in Table 9. The most accurate response was based on beam theory (Choi et al., 2006). It is evident that SSQ14 and SSQ18 provided accurate responses for both regular and distorted mesh.

Thin Cantilever Beam under In-Plane Shear

A cantilever beam with a length of 100, width of 1, and thickness of 1 is shown in Figure 10. The modulus of elasticity is 1000000 and the Poisson's ratio is 0.3. A force of 1 at the free end is a strong test for the structure. A mesh size of 1×100 is employed for analysis of the cantilever beam. The number of parts in the x and y directions are 100 and 1, respectively. In this size mesh, the aspect ratios of the elements are equal to one. Size 2×100 mesh was also used. The exact displacements of the beam's free end in the x and y directions are 0.03 and 4, respectively (Wisniewski and Turska, 2009).
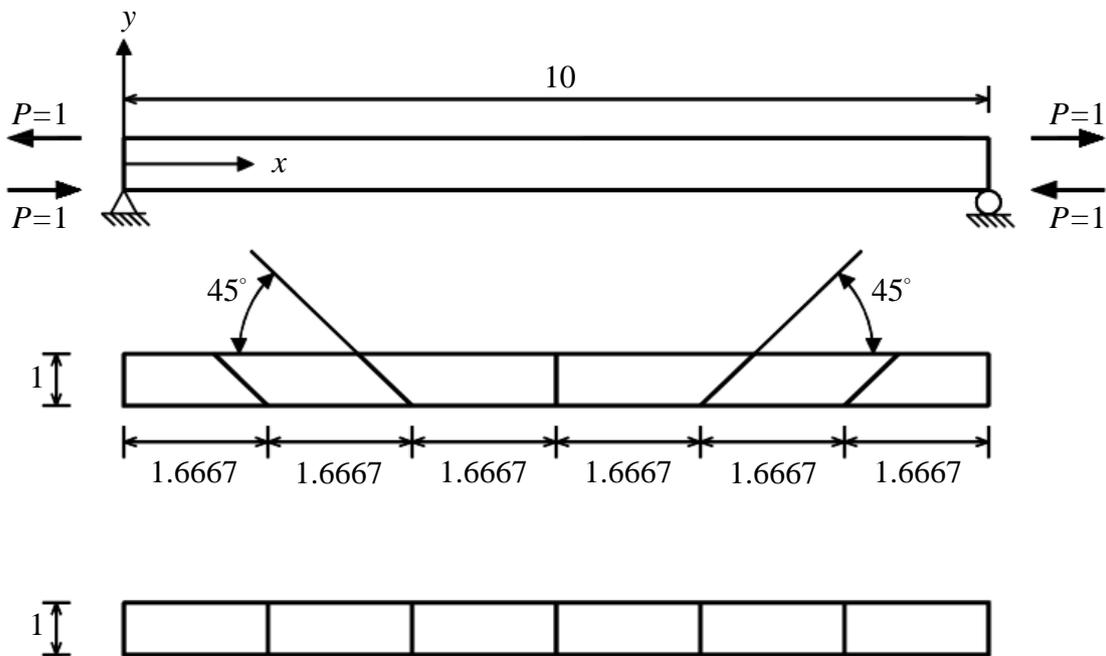

Fig. 9. The loading and meshes of the straight beam under pure bending.

Table 9. The displacement of the beam under pure bending.

Elements	Regular Mesh		Distorted Mesh	
	Maximum u_x	Maximum u_y	Maximum u_x	Maximum u_y
ALLMAN	-0.6	1.5	-0.498	1.215
QM6	-0.6	1.5	-0.554	1.384
IB	-0.6	1.5	-0.459	1.124
SSQUAD	-0.6	1.5	-0.6	1.5
SSQ14	-0.6	1.5	-0.6	1.5
SSQ18	-0.6	1.5	-0.6	1.5
Exact (Choi et al., 2006)	-0.6	1.5	-0.6	1.5

The responses of good elements are shown in Table 10 and it can be seen that the solution errors for SSQ18 were very low. The number of errors for SSQ14 in 2×100 mesh increased because of the rotational DOF and equilibrium condition being satisfied in the domain of the second-order field.

Cantilever Beam with Irregular Mesh

Figure 11 shows the geometric properties, loading and 5-element mesh. The modulus of elasticity is 1500 and the Poisson's ratio is 0.25 without the unit. Two loading cases are employed for analysis: a pure bending under the bending moment of M and linear bending under the concentrated force of P. Real vertical displacements of the beam at point A for M and P loading are 100.00 and 102.60, respectively (Cen et al., 2009).

The structure was analyzed using irregular 5-element mesh (Figure 11). The responses of elements of other researchers were used as a basis of comparison. Table 11 compares the results of the various elements for the two types of loading and show that errors for SSQ14 and SSQ18 were only 1.5% for the pure bending case. The response error for SSQ18 and SSQ14 for P loading were 0.9% and 1.5%.
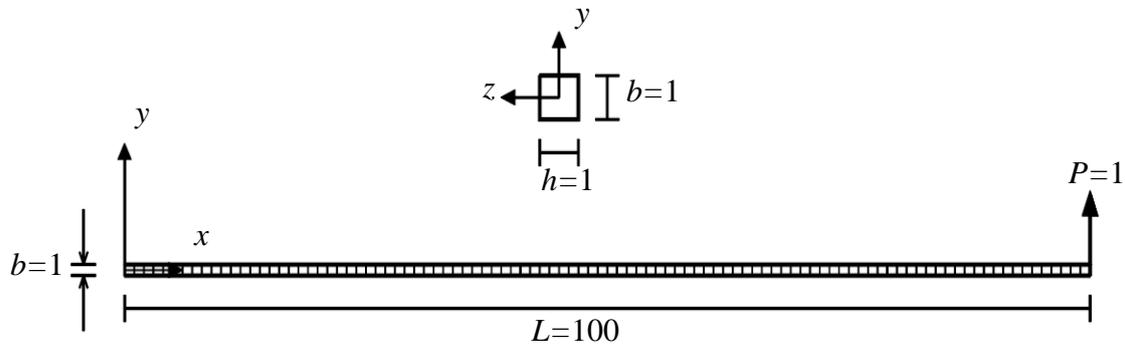

Fig. 10. The geometry of the thin cantilever beam under in-plane shear.

Table 10. The displacement of the free end of the thin cantilever beam under in-plane shear.

| Elements	Mesh	$u_x \times 100$	u_y
HW14-S, HW14-N, HW18	1×100	3	4.0002
	2×100	2.9988	3.9978
HW12-S, HW10-N	1×100	2.73	3.6402
	2×100	2.9264	3.9013
Q4	1×100	2.0222	2.6965
	2×100	2.128	2.8371
EADG4, HR5-S	1×100	3	4.0002
	2×100	2.9988	3.9978
SSQUAD	1×100	3.004621	4.006691
	2×100	2.999078	3.998181
SSQ14	1×100	3.000006	4.000242
	2×100	3.193297	4.258160
SSQ18	1×100	2.998288	3.996738
	2×100	2.998900	3.998032
Reference value(Wisniewski and Turska, 2009)		3	4
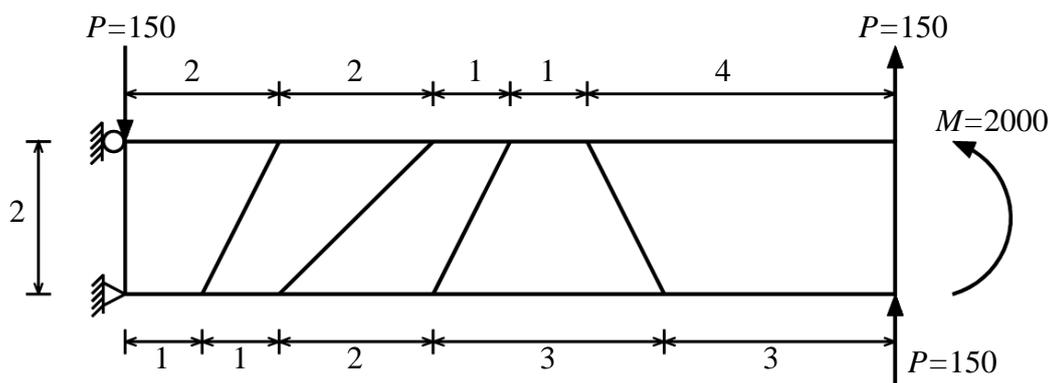
Fig. 11. The cantilever beam with irregular mesh.

Table 11. The displacement of the cantilever beam in two loading cases.

Elements	M	P
Q6	98.40	100.40
QM6	96.07	97.98
NQ6	96.10	98.00
PS	96.18	98.05
QE-2	96.50	98.26
B-Q4E	96.5	98.26
AGQ6-II	100.0	102.7
QACM4	96.0	98.0
QAC-ATF4	100.0	102.4
Q8	99.7	101.5
QACM8	101.3	102.8
SSQUAD	100.00	102.79
SSQ14	101.66	104.16
SSQ18	101.48	103.52
Exact(Cen et al., 2009)	100.00	102.60

Cantilever beam with four-element

In the mesh of the cantilever beam of this test, 4 irregular Cantilever beam with 4 elements quadrilateral elements are used. The geometry of the beam is shown in Figure 12. The modulus of elasticity is 30000, the Poisso's ratio is 0.25, and the thickness of the beam is 1. The free end of the beam is under a parabolic distributed shear load. The vertical displacement at points A and B are listed in Table 12. The displacement of the beam at both A and B points is equal to 0.3558 (Cen et al., 2009). This test evaluates the capability of the elements for shear deformations for an irregular mesh. The low error of the SSQ14 and SSQ18 elements is evident in

Table 12. These errors for SSQ18 and SSQ14 elements were 1% and 0.03%.

Thick Curved Beam

A thick curved beam is analyzed in Figure 13 under a shear force of 600 on the free end. The modulus of elasticity is 1000, Poisson's ratio is 0, and the thickness of the structure 1. A 4-element mesh is used for analysis. The vertical displacement at point A is listed in Table 13. The accurate response for vertical displacement at point A is 90.1 (Cen et al., 2007). The response error for SSQ14 and SSQ18 was 3.5% and 4%, respectively.

150
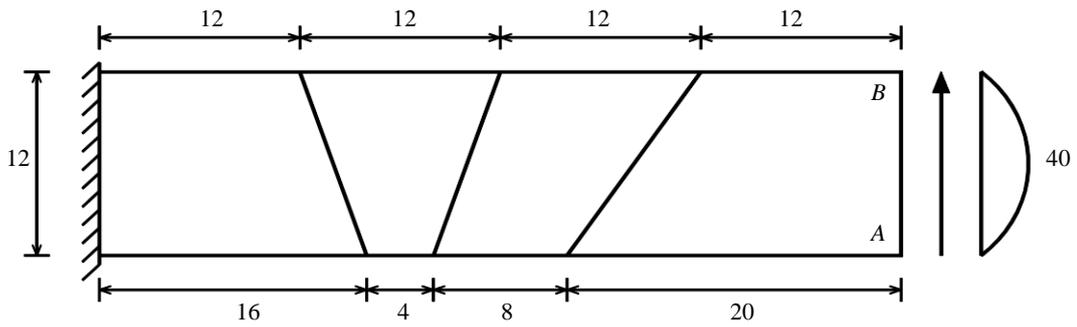
Fig. 12. The cantilever beam with four-element.

Table 12. The displacement of the cantilever beam under the shear parabolic distributed load on the free end.

Elements	Tip Deflection		
	Point A	Point B	Average
Q4S	-	-	0.2978
D-type	-	-	0.3065
Q6	0.3395	0.3409	0.3402
QM6	0.3264	0.3286	0.3275
AGQ6-II	0.3535	0.3530	0.3533
QACM4	0.3280	0.3305	0.3293
QAC-ATF4	0.3523	0.3516	0.3520
Q8	0.3481	0.3474	0.3479
QACM8	0.3524	0.3517	0.3520
CQAC-Q8	0.3529	0.3520	0.3524
SSQUAD	0.3530	0.3525	0.3528
SSQ14	0.3559	0.3559	0.3559
SSQ18	0.3526	0.3520	0.3523
Exact(Cen et al., 2009)		0.3558	
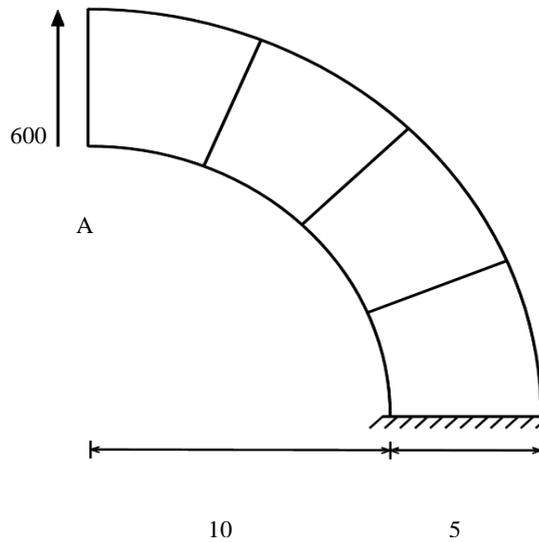
Fig. 13. The geometry and loading of the thick curved beam.

Table 13. The displacement of the point A in the thick curved beam under shear force at its free end.

Elements	QM6	PS	PEAS7	QAC-ATF4	AGQ6-II	QACM4	Q8	QACM8	SSQUAD	SSQ14	SSQ18	Exact (Cen et al., 2007)
Deflection	83.61	84.58	84.58	90.6	86.90	84.59	88.6	84.1	86.92	87.00	86.45	90.1

Thin Curved Beam

Figure 14 shows the geometry of a thin curved beam with a fixed end. The other end is subjected to a shear force of 1. The modulus of elasticity is 10000000, Poisson's ratio is 0.25, and the beam thickness is 0.1. The real vertical displacement under the load is 0.08734

(Choo et al., 2006). Table 14 lists the responses for vertical displacement for the different elements. SSQ18 provided the best answer of all good elements. In coarse mesh, the response of SSQ14 showed very low error, but as the mesh became finer, error increased to 2%.
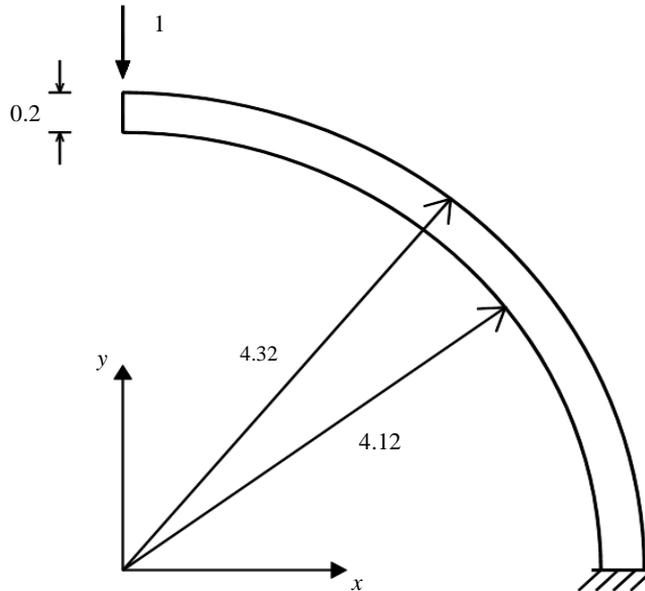
Fig. 14. The geometry of the thin curved beam under shear force on its free end.

Table 14. The vertical displacement of the thin curved beam under the load.

Elements	HT	ALLMAN	MEAS	HTD	Q8	SSQUAD	SSQ14	SSQ18	Near Exact (Fu et al., 2010)
6×1	-0.00662	-0.07756	-0.07756	-0.08420	-0.08759	-0.08901	-0.08748	-0.08745	
12×2	-0.02201	-0.08736	-0.08736	-0.08808	-	-0.08844	-0.08895	-0.08840	-0.0886
24×4	-0.04850	-0.08808	-0.08827	-0.08843	-	-0.08846	-0.08925	-0.08850	

Thick-Walled Cylinder

To investigate the behavior of nearly incompressible materials, a plane strain problem for a thick-walled cylinder under an internal pressure of one was analyzed. Symmetry requires that only 1/4 of the cylinder be used. Figure 15 shows the geometry and mesh of the structure. The modulus of elasticity is 1000 and the inner and outer radii of the cylinder are 3 and 9, respectively. The central angle is divided into 9 parts, each equal to 10%. The details of meshing are shown in Figure 15b. The

measurements of the parts of the radius are also given in Figure 15b. Normalized radius displacement of the inner surface by variation in the Poisson's ratio is shown in Table 15. Accurate displacement for each Poisson's ratio is recorded in the last row of the table. The responses of the other good elements were used for comparison. Table 15 shows that the responses for SSQ18 and SSQ14 were insensitive to variation in the Poisson's ratio. The response error for SSQ18 and SSQ14 were 4% and 18%, respectively.

(1)   (2)
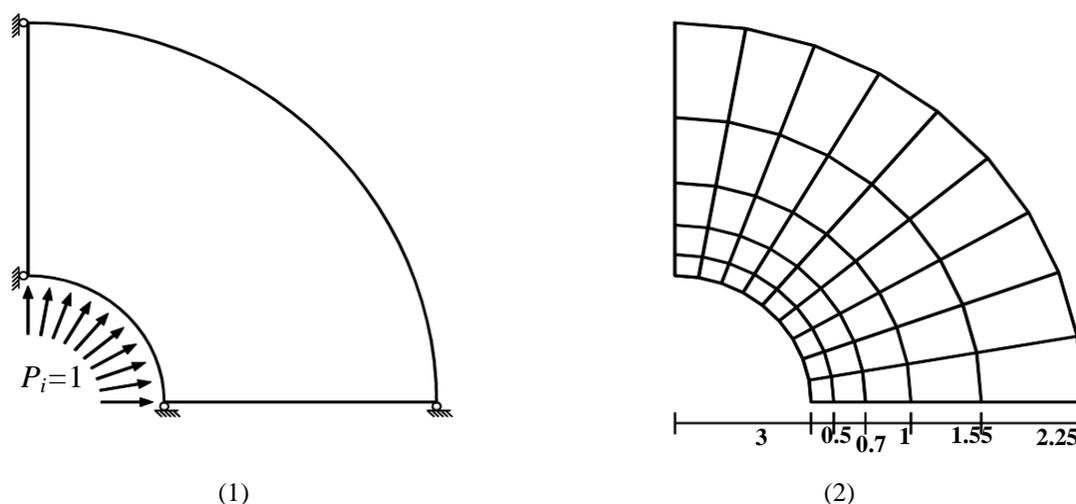
Fig. 15. The loading and mesh of the thick walled cylinder under internal pressure.

Table 15. The normalized displacement in the thick walled cylinder under internal pressure.

ν	0.3	0.49	0.499	0.4999
HT	1.01092	1.02976	1.03162	1.03162
CQUAD4	0.99563	0.99206	0.99012	0.99209
ALLMAN	1.13537	0.91270	0.37154	0.05736
MEAS	0.99563	0.99206	0.99012	0.99209
HTD	1.01092	1.02976	1.03162	1.03162
SSQUAD	0.97988	0.97894	0.97903	0.97942
SSQ14	1.18049	1.18388	1.18412	1.18461
SSQ18	0.93602	0.95767	0.95928	0.95988
Exact (Choo et al., 2006)	0.00458	0.00504	0.00506	0.00506

CONCLUSIONS

Utilizing the free formulation and the strain gradient notation methods, quadrilateral elements SSQ14 and SSQ18 were created and tested. These elements were obtained based on the complete second-order function for strain. This kind of the field guarantees fulfillment of Felippa's pure bending test, rotational invariance and absence of parasitic shear error. Moreover, this study makes use of the equilibrium equations in perfect and imperfect forms. Establishing equilibrium condition decreases the number of the strain states required in the formulation.

The numerical results showed that the establishment of equilibrium equations only for the linear part of the strain field leads to more accurate responses than for the complete equilibrium equations for the second-order strain field. Based on results of numerical tests, SSQ14 was shown to provide larger responses when the mesh is refined. This study indicates that using rotational DOF and satisfying the equilibrium condition in the domain of the second-order field decreased the ability of this element.

The efficient SSQ18 element has all the good characteristics of the SSQUAD element. Furthermore, the responses for SSQ18 in the strong patch tests of constant stress and bending with bilinear stress showed good accuracy, even for substantial mesh distortion. These strong patch tests can result in many errors when good elements, such as SSQUAD and AGQ6-II, are utilized. Several difficult numerical tests were used to illustrate the accurate performance of SSQ18. It was shown that SSQ14 provided high-quality responses in most of these experiments.

Appendix A

The stress contours for the Cook's trapezoidal cantilever beam are provided here. The following contours show the stresses of σ_x, σ_y and τ_{xy} for a 4×4 mesh for elements SSQ18 and SSQ14.
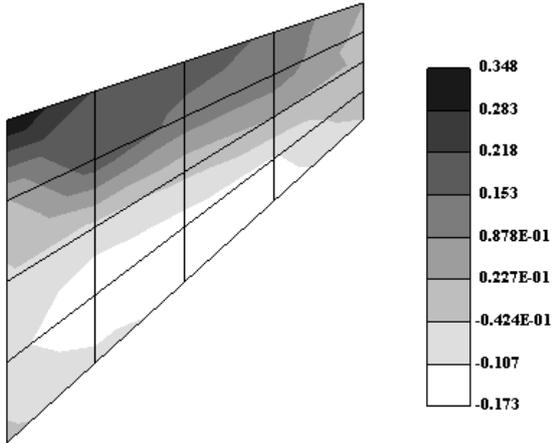

Fig. 16. Stress contours for σ_x in SSQ18.
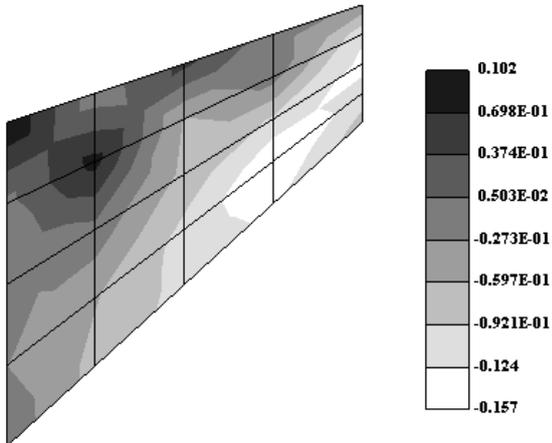
Fig. 17. Stress contours for σ_y in SSQ18.
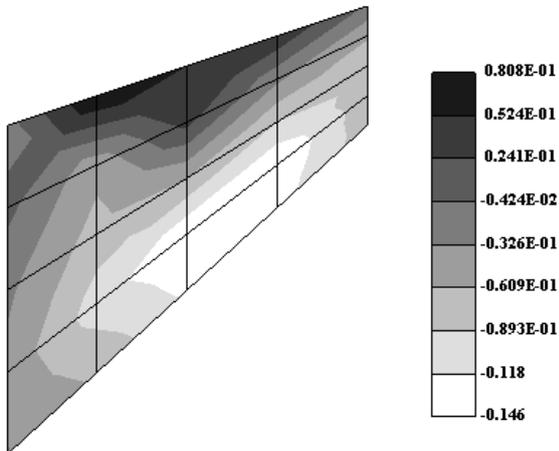
Fig. 18. Stress contours for τ_{xy} in SSQ18.
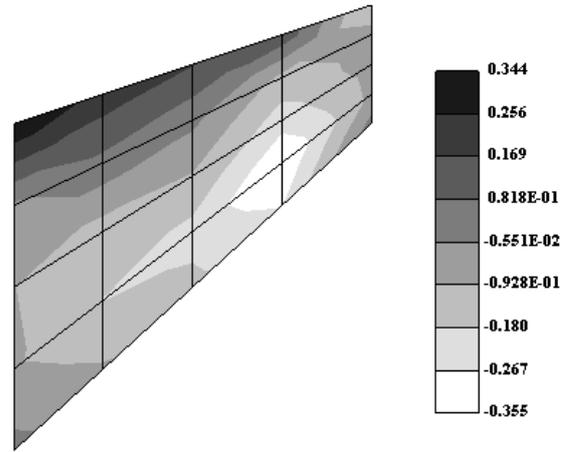
Fig. 19. Stress contours for σ_x in SSQ14.
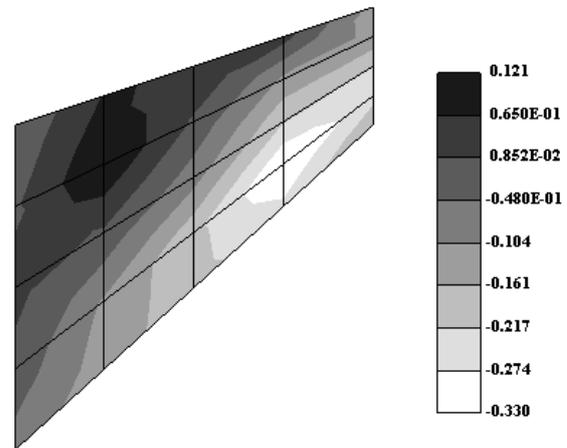

**Fig. 20.** Stress contours for σ_y in SSQ14.
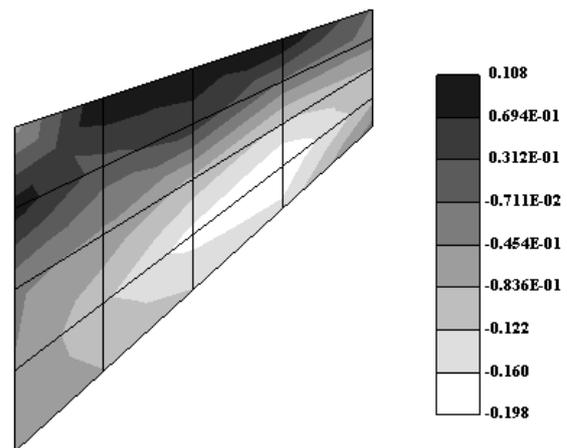
Fig. 21. Stress contours for τ_{xy} in SSQ14.

REFERENCES

Allman, D.J. (1984). "A compatible triangular element including vertex rotations for plane elasticity analysis", *Computers and Structures*, 19(1-2), 1-8.

Andelfinger, U. and Ramm, E. (1993). "EAS-elements for two-dimensional, three-dimensional, plate and shell structures and their equivalence to HR-elements", *International Journal for Numerical Methods in Engineering*, 36(8), 1311-1337.

Bergan, P.G. and Felippa, C.A. (1985). "A triangular membrane element with rotational degrees of freedom", *Computer Methods in Applied Mechanics and Engineering*, 50(1), 25-69.

Cen, S. Chen, X.M. and Fu, X.R. (2007). "Quadrilateral membrane element family formulated by the quadrilateral area coordinate method", *Computer Methods in Applied Mechanics and Engineering*, 196(41-44), 4337-4353.

Cen, S. Chen, X.M. Li, C.F. and Fu, X.R. (2009). "Quadrilateral membrane elements with analytical element stiffness matrices formulated by the new quadrilateral area coordinate method (QACM-II)", *International Journal for Numerical Methods in Engineering*, 77(8), 1172-1200.

Chen, X.M. Cen, S. Long, Y.Q. and Yao, Z.H. (2004). "Membrane elements insensitive to distortion using the quadrilateral area coordinate method", *Computers and Structures*, 82(1), 35-54.

Choi, N. Choo, Y.S. and Lee, B.C. (2006). "A hybrid Trefftz plane elasticity element with drilling degrees of freedom", *Computer Methods in Applied Mechanics and Engineering*, 195(33-36), 4095-4105.

Choo, Y.S. Choi, N. and Lee, B.C. (2006). "Quadrilateral and triangular plane elements with rotational degrees of freedom based on the hybrid Trefftz method", *Finite Elements in Analysis and Design*, 42(11), 1002-1008.

Cook, R.D. Malkus, D.S. and Plesha, M.E. (1989). *Concepts and Applications of Finite Element Analysis*, 3rd Edition, Wiley, New York.

Cook, R.D. (1974). "Improved two-dimensional finite element", *Journal of the Structural Division, ASCE,* 100(ST6), 1851-1863.

Cook, R.D. (1986). "On the Allman triangle and a related quadrilateral element", *Computers and Structures*, 22(6), 1065-1067.

Dow, J.O. (1999). *A unified approach to the Finite Element method and error analysis procedures*, Academic Press.

Felippa, C.A. and Militello, C. (1990). "The variational formulation of high performance finite elements: parametrized variational principles", *Computers and Structures*, 36(1), 1-11.

Felippa, C.A. (2000). "Recent advances in finite element templates (Chapter 4)", In: Topping, B.H.V. (Ed.), *Computational Mechanics for the Twenty-First Century*, pp. 71-98, Saxe-Coburn Publications, Edinburgh.

Felippa, C.A. (2003). "A study of optimal membrane triangles with drilling freedoms", *Computer Methods in Applied Mechanics and Engineering*, 192(16-18), 2125-2168.

Felippa, C.A. (2004). "A template tutorial", In: Mathisen, K.M., Kvamsdal, T., Okstad, K.M. (Eds.), *Computational Mechanics: Theory and Practice, CIMNE*, Barcelona, 29-68.

Felippa, C.A. (2006). "Supernatural QUAD4: a template formulation", invited contribution to J.H. Argyris Memorial Issue, *Computer Methods in Applied Mechanics and Engineering*, 195(41-43), 5316-5342.

Fu, X.R. Cen, S. Li, C.F. and Chen, X.M. (2010). "Analytical trial function method for development of new 8-node plane element based on the variational principle containing Airy stress function", *Engineering Computations*, 27(4), 442-463.

Ibrahimgovic, A. Taylor, R.L. and Wilson, E.L. (1990). "A robust quadrilateral membrane finite element with rotational degrees of freedom", *International Journal for Numerical Methods in Engineering*, 30(3), 445-457.

Jirousek, J. and Venkatesh, A. (1992). "Hybrid Trefftz plane elasticity elements with p method capabilities", *International Journal for Numerical Methods in Engineering*, 35(7), 1443-1472.

Long, Y.Q. and Xu, Y. (1994). "Generalized conforming quadrilateral membrane element with vertex rigid rotational freedom", *Computers and Structures*, 52(4), 749-755.

Long, Z.F. Cen, S. Wang, L. Fu, X.R. and Long, Y.Q. (2010). "The third form of the quadrilateral area coordinate method (QACM-III): theory, application, and scheme of composite coordinate interpolation", *Finite Elements in Analysis and Design,* 46(10), 805-818.

MacNeal, R.H. and Harder, R.L. (1985). "A proposed standard set of problems to test finite element accuracy", *Finite Elements in Analysis and Design*, 1(1), 3-20.

MacNeal, R.H. and Harder, R.L. (1988). "A refined four-node membrane element with rotation degrees of freedom", *Computers and Structures*, 28(1), 75-84.

MacNeal, R.H. (1971). *The nastran theoretical manual*, NASA-SP-221(01).

Nygard, M.K. (1986). *The free formulation for nonlinear finite elements with applications to shells*, Ph.D. Dissertation, Division of Structural Mechanics, NTH, Trondheim, Norway.

Paknahad, M. Noorzaei, J. Jaafar, M.S. and Thanoon, W.A. (2007). "Analysis of shear wall structure using optimal membrane triangle element", *Finite Elements in Analysis and Design*, 43(11-12), 861-869.

Pian, T.H.H. and Sumihara, K. (1984). "Rational approach for assumed stress finite elements", *International Journal for Numerical Methods in Engineering*, 20(9), 1685-1695.

Piltner, R. and Taylor, R.L. (1995). "A quadrilateral mixed finite element with two enhanced strain modes", *International Journal for Numerical Methods in Engineering*, 38(11), 1783-1808.

Piltner, R. and Taylor, R.L. (1997). "A systematic constructions of B-bar functions for linear and nonlinear mixed-enhanced finite elements for plane elasticity problems", *International Journal for Numerical Methods in Engineering*, 44(5), 615-639.

Prathap, G. and Senthilkumar, V. (2008). "Making sense of the quadrilateral area coordinate membrane elements", *Computer Methods in Applied Mechanics and Engineering*, 197(49-50), 4379-4382.

Rezaiee-Pajand, M. and Yaghoobi, M. (2012). "Formulating an effective generalized four-sided element", *European Journal of Mechanics A/Solids*, 36, 141-155.

Santos, H.A.F.A. and Moitinho de Almeida, J.P. (2014). "A family of Piola–Kirchhoff hybrid stress finite elements for two-dimensional linear elasticity", *Finite Elements in Analysis and Design*, 85, 33–49.

Taylor, R.L. Beresford, P.J. and Wilson, E.L. (1976). "A non-conforming element for stress analysis", *International Journal for Numerical Methods in Engineering*, 10(6), 1211-1219.

Wilson, E.L. Taylor, R.L. Doherty, W.P. and Ghabussi, T. (1973). "Incompatible displacement models", In: Fenven, S.T., et al. (Eds.), *Numerical and Computer Methods in Structural Mechanics*, pp. 43-57, Academic Press, New York.

Wisniewski, K. and Turska, E. (2006). "Enhanced Allman quadrilateral for finite drilling Rotations", *Computer Methods in Applied Mechanics and Engineering*, 195(44-47), 6086-6109.

Wisniewski, K. and Turska, E. (2008). "Improved four-node Hellingere Reissner elements based on skew coordinates", *International Journal for Numerical Methods in Engineering*, 76(6), 798-836.

Wisniewski, K. and Turska, E. (2009). "Improved 4-node Hu-Washizu elements based on skew coordinates", *Computers and Structures*, 87(7-8), 407-424.

Wu, C.C. Huang, M.G. and Pian, T.H.H. (1987). "Consistency condition and convergence criteria of incompatible elements: general formulation of incompatible functions and its application", *Computers and Structures*, 27(5), 639-644.

Yeo, S.T. and Lee, B.C. (1997). "New stress assumption for hybrid stress elements and refined four-node plane and eight-node brick elements", *International Journal for Numerical Methods in Engineering*, 40(16), 2933-2952.